JHEP

Published for SISSA by Springer

Received: October 22, 2013
Revised: December 1, 2013
Accepted: December 8, 2013
Published: January 16, 2014

JHEP01(2014)077

Beam-helicity asymmetry in associated electroproduction of real photons $ep \to e\gamma\pi N$ in the Δ-resonance region

The HERMES collaboration

DESY – HERMES, Notkestraße 85, D-22607 Hamburg

E-mail: management@hermes.desy.de

Abstract: The beam-helicity asymmetry in associated electroproduction of real photons, $ep \to e\gamma\pi N$, in the $\Delta(1232)$-resonance region is measured using the longitudinally polarized Hera positron beam and an unpolarized hydrogen target. Azimuthal Fourier amplitudes of this asymmetry are extracted separately for two channels, $ep \to e\gamma\pi^0 p$ and $ep \to e\gamma\pi^+ n$, from a data set collected with a recoil detector. All asymmetry amplitudes are found to be consistent with zero.

Keywords: Lepton-Nucleon Scattering, QCD, Polarization, Photon production

ArXiv ePrint: 1310.5081

doi:10.1007/JHEP01(2014)077

The HERMES collaboration

A. Airapetian [13,16], N. Akopov [27], E.C. Aschenauer [7], W. Augustyniak [26], R. Avakian [27], A. Avetissian [27], E. Avetisyan [6], H.P. Blok [18,25], H. Böttcher [7], A. Borissov [6], J. Bowles [14], I. Brodski [13], V. Bryzgalov [20], J. Burns [14], G.P. Capitani [11], E. Cisbani [22], G. Ciullo [10], M. Contalbrigo [10], P.F. Dalpiaz [10], W. Deconinck [6], R. De Leo [2], E. De Sanctis [11], M. Diefenthaler [15,9], P. Di Nezza [11], M. Düren [13], M. Ehrenfried [13], G. Elbakian [27], F. Ellinghaus [5], E. Etzelmüller [13], R. Fabbri [7], S. Frullani [22], G. Gapienko [20], V. Gapienko [20], J. Garay García [4], F. Garibaldi [22], G. Gavrilov [6,19,23], V. Gharibyan [27], F. Giordano [15,10], S. Gliske [16], M. Hartig [6], D. Hasch [11], Y. Holler [6], I. Hristova [7], A. Ivanilov [20], H.E. Jackson [1], S. Joosten [12,15], R. Kaiser [14], G. Karyan [27], T. Keri [14,13], E. Kinney [5], A. Kisselev [19], V. Korotkov [20], V. Kozlov [17], P. Kravchenko [9,19], V.G. Krivokhijine [8], L. Lagamba [2], L. Lapikás [18], I. Lehmann [14], P. Lenisa [10], W. Lorenzon [16], X.-G. Lu [6], B.-Q. Ma [3], D. Mahon [14], N.C.R. Makins [15], S.I. Manaenkov [19], Y. Mao [3], B. Marianski [26], H. Marukyan [27], C.A. Miller [23], Y. Miyachi [24], A. Movsisyan [10], V. Muccifora [11], M. Murray [14], A. Mussgiller [6,9], Y. Naryshkin [19], A. Nass [9], M. Negodaev [7], W.-D. Nowak [7], L.L. Pappalardo [10], R. Perez-Benito [13], A. Petrosyan [27], P.E. Reimer [1], A.R. Reolon [11], C. Riedl [15,7], K. Rith [9], G. Rosner [14], A. Rostomyan [6], J. Rubin [1,15], D. Ryckbosch [12], Y. Salomatin [20], A. Schäfer [21], G. Schnell [4,12], B. Seitz [14], T.-A. Shibata [24], M. Stahl [13], M. Statera [10], E. Steffens [9], J.J.M. Steijger [18], J. Stewart [7], F. Stinzing [9], S. Taroian [27], A. Terkulov [17], R. Truty [15], A. Trzcinski [26], M. Tytgat [12], Y. Van Haarlem [12], C. Van Hulse [4,12], V. Vikhrov [19], I. Vilardi [2], S. Wang [3], S. Yaschenko [6,7,9], Z. Ye [6], S. Yen [23], V. Zagrebelnyy [6,13], B. Zihlmann [6], P. Zupranski [26]

[1] *Physics Division, Argonne National Laboratory, Argonne, Illinois 60439-4843, USA*
[2] *Istituto Nazionale di Fisica Nucleare, Sezione di Bari, 70124 Bari, Italy*
[3] *School of Physics, Peking University, Beijing 100871, China*
[4] *Department of Theoretical Physics, University of the Basque Country UPV/EHU, 48080 Bilbao, Spain and IKERBASQUE, Basque Foundation for Science, 48011 Bilbao, Spain*
[5] *Nuclear Physics Laboratory, University of Colorado, Boulder, Colorado 80309-0390, USA*
[6] *DESY, 22603 Hamburg, Germany*
[7] *DESY, 15738 Zeuthen, Germany*
[8] *Joint Institute for Nuclear Research, 141980 Dubna, Russia*
[9] *Physikalisches Institut, Universität Erlangen-Nürnberg, 91058 Erlangen, Germany*
[10] *Istituto Nazionale di Fisica Nucleare, Sezione di Ferrara and Dipartimento di Fisica e Scienze della Terra, Università di Ferrara, 44122 Ferrara, Italy*
[11] *Istituto Nazionale di Fisica Nucleare, Laboratori Nazionali di Frascati, 00044 Frascati, Italy*
[12] *Department of Physics and Astronomy, Ghent University, 9000 Gent, Belgium*
[13] *II. Physikalisches Institut, Justus-Liebig Universität Gießen, 35392 Gießen, Germany*
[14] *SUPA, School of Physics and Astronomy, University of Glasgow, Glasgow G12 8QQ, United Kingdom*
[15] *Department of Physics, University of Illinois, Urbana, Illinois 61801-3080, USA*
[16] *Randall Laboratory of Physics, University of Michigan, Ann Arbor, Michigan 48109-1040, USA*
[17] *Lebedev Physical Institute, 117924 Moscow, Russia*
[18] *National Institute for Subatomic Physics (Nikhef), 1009 DB Amsterdam, The Netherlands*
[19] *B.P. Konstantinov Petersburg Nuclear Physics Institute, Gatchina, 188300 Leningrad Region, Russia*
[20] *Institute for High Energy Physics, Protvino, 142281 Moscow Region, Russia*
[21] *Institut für Theoretische Physik, Universität Regensburg, 93040 Regensburg, Germany*
[22] *Istituto Nazionale di Fisica Nucleare, Sezione di Roma, Gruppo Collegato Sanità and Istituto Superiore di Sanità, 00161 Roma, Italy*
[23] *TRIUMF, Vancouver, British Columbia V6T 2A3, Canada*
[24] *Department of Physics, Tokyo Institute of Technology, Tokyo 152, Japan*
[25] *Department of Physics and Astronomy, VU University, 1081 HV Amsterdam, The Netherlands*
[26] *National Centre for Nuclear Research, 00-689 Warsaw, Poland*
[27] *Yerevan Physics Institute, 375036 Yerevan, Armenia*

JHEP01(2014)077

Contents

1 Introduction

There continues to be intense interest in Generalized Parton Distributions (GPDs) [1–3], both theoretical and experimental. These distributions relate to the total angular momentum of partons in the nucleon [4] and information on the parton's transverse location in the nucleon correlated with the fraction of the nucleon's longitudinal momentum carried by that parton [5]. The GPDs that have thus far attracted the most interest parametrize the nonperturbative part of hard exclusive reactions where the target system stays intact such as $ep \to e\gamma p$. They depend on four kinematic variables: t, x, ξ, and Q^2. The Mandelstam variable $t = (p - p')^2$ is the square of the difference between the initial (p) and final (p') four-momenta of the target nucleon. The variable x is the average of the initial and final fractions of the (large) target longitudinal momentum that is carried by the struck parton, and the variable ξ, known as the skewness, is half of the difference between these fractions. The evolution of GPDs with the photon virtuality $Q^2 \equiv -q^2$ is analogous to that of parton distribution functions, with $q = k - k'$ being the difference between the four-momenta of the incident and the scattered leptons. Currently, no hard exclusive measurements exist that provide access to x. Because of the lack of consensus about the definition of ξ in terms of experimental observables, the results are typically reported by HERMES as projections in $x_{\mathrm{B}} \equiv Q^2/(2pq)$, to which ξ can be related through $\xi \simeq x_{\mathrm{B}}/(2 - x_{\mathrm{B}})$ in the generalized Bjorken limit of large Q^2 and fixed x_{B} and t. Several GPDs describe various possible helicity transitions of the struck quark and/or the nucleon. At leading twist (i.e., twist-2) and for a spin-1/2 target such as the proton, four chiral-even GPDs (H^q, $\widetilde{H}^q$, E^q, $\widetilde{E}^q$) are required to describe processes that conserve the helicity of the struck quark with flavor q.

JHEP01(2014)077

The GPD formalism can be extended to more general baryonic final states, in particular here to the Δ resonance. Similar to $N \to \Delta$ "transition" form factors, one can introduce $N \to \Delta$ transition GPDs. At leading twist, the $\gamma^* N \to \gamma\Delta$ process can be parametrized in terms of three vector and four axial-vector $N \to \Delta$ GPDs [6]. Among them, one expects three such GPDs to dominate at small $|t|$: the magnetic vector GPD H_M, of which the first moment corresponds to the $N \to \Delta$ magnetic dipole transition form factor $G_M^*(t)$, and the axial-vector GPDs C_1 and C_2, of which the first moments correspond to the axial-vector and pseudoscalar $N \to \Delta$ form factors, respectively.

In ref. [7], a model is proposed to describe the "associated" reaction $ep \to e\gamma\pi N$. In this model, the so-called soft-pion technique that is based on current algebra and chiral symmetry allows for S-wave pions the use of the same GPDs as in $ep \to e\gamma p$. In order to extend the model estimations to pions of higher energy, the P-wave production is assumed to be dominated by the $\Delta(1232)$ isobar production and is added following the large N_c limit approach for $N \to \Delta$ GPDs developed in refs. [6, 8]. In this model, the $N \to \Delta$ GPDs H_M, C_1, and C_2 are connected to the $N \to N$ isovector GPDs as:

$$\begin{aligned} H_M(x,\xi,t) &= \frac{2}{\sqrt{3}}\left[E^u(x,\xi,t) - E^d(x,\xi,t)\right], \\ C_1(x,\xi,t) &= \sqrt{3}\left[\widetilde{H}^u(x,\xi,t) - \widetilde{H}^d(x,\xi,t)\right], \\ C_2(x,\xi,t) &= \frac{\sqrt{3}}{4}\left[\widetilde{E}^u(x,\xi,t) - \widetilde{E}^d(x,\xi,t)\right]. \end{aligned} \tag{1.1}$$

This estimate is expected to have an accuracy of about 30%. Thus, these large N_c relations allow the interpretation of the associated reaction in terms of nucleon GPDs and therefore open (model-dependent) access to different flavor combinations of the nucleon GPDs. For example, $ep \to e\gamma p$ is sensitive to the combination $\frac{4}{9}\widetilde{H}^u + \frac{1}{9}\widetilde{H}^d$, whereas in $ep \to e\gamma\Delta$ the isovector part $\widetilde{H}^u - \widetilde{H}^d$ appears.

As for the $ep \to e\gamma p$ reaction, for the associated reaction the amplitudes of the Deeply Virtual Compton Scattering (DVCS) process and of the Bethe-Heitler (BH) process, in which a bremsstrahlung photon is radiated from the incident or scattered lepton, combine coherently. In the absence of available data for the associated reaction, the pion photoproduction cross section calculated using an approach similar to that applied to the associated BH process is compared in ref. [7] with experimental data from refs. [9–11]. Around the Δ-resonance mass, the model overestimates the experimental cross sections by about 10%.

In this paper, the first measurement of the single-charge beam-helicity asymmetry in the reaction $ep \to e\gamma\pi N$ is presented and compared with model predictions. The asymmetry is defined as in ref. [12] to be

$$\mathcal{A}_{\mathrm{LU}}(\phi, e_\ell) = \frac{\sigma_{\mathrm{LU}}(\phi, e_\ell, \lambda = +1) - \sigma_{\mathrm{LU}}(\phi, e_\ell, \lambda = -1)}{\sigma_{\mathrm{LU}}(\phi, e_\ell, \lambda = +1) + \sigma_{\mathrm{LU}}(\phi, e_\ell, \lambda = -1)}. \tag{1.2}$$

Here, σ_{LU} denotes the differential cross section for longitudinally polarized beam and unpolarized target, $\lambda = \pm 1$ and $e_\ell (= +1)$ are respectively the helicity and unit charge of the beam lepton, and the angle ϕ is the azimuthal orientation of the photon production plane with respect to the lepton scattering plane. The definition of the angle ϕ follows the Trento

JHEP01(2014)077

conventions [13]. The asymmetries are extracted in the kinematic range of $-t < 1.2\,\mathrm{GeV}^2$, $0.03 < x_B < 0.35$, and $1\,\mathrm{GeV}^2 < Q^2 < 10\,\mathrm{GeV}^2$.

2 The HERMES experiment in 2006–2007

The data presented here were collected in 2006 and 2007 at HERMES (DESY) using the 27.6 GeV HERA positron beam and an unpolarized hydrogen gas target internal to the beam line. For this measurement, the recoil detector [14] was used in conjunction with the forward spectrometer [15].

The HERA lepton beam was transversely self-polarized by the emission of synchrotron radiation [16]. Longitudinal polarization of the beam in the target region was achieved by a pair of spin rotators located upstream and downstream of the experiment [17]. The sign of the beam polarization was reversed three times over the running period. Two Compton backscattering polarimeters [**?** **?**] independently measured the longitudinal and transverse beam polarizations.

For the analysis of the beam-helicity asymmetry considered here, data collected with only one lepton beam charge ($e_\ell = +1$) and both beam-helicity states are available. For this data set, the average beam polarization was $P_\ell = 0.402$ (-0.394) for positive (negative) beam helicity, with a total relative uncertainty of 1.96% [20].

The scattered lepton and particles produced in the polar-angle range 0.04 rad $< \theta <$ 0.22 rad were detected by the forward spectrometer, for which the average lepton-identification efficiency was at least 98% with hadron contamination of less than 1%. The produced particles emerging at large polar angles and with small momenta were detected by the recoil detector in the polar-angle range 0.25 rad $< \theta <$ 1.45 rad, with an azimuthal coverage of about 75%. The lower-momentum detection threshold for protons (pions) was 125 (60) MeV for this analysis.

The recoil detector surrounded the target cell and consisted of a Silicon Strip Detector (SSD), a Scintillating Fiber Tracker (SFT), and a photon detector, all embedded in a solenoidal magnetic field with field strength of 1 T. A detailed description of the recoil-detector components is given in ref. [14].

Track search and momentum reconstruction in the recoil detector are performed by combining coordinate information from the SSD and SFT layers. For protons, energy deposition in the SSD is additionally taken into account. This improves the momentum resolution for momenta below 0.5 GeV, leading to a resolution of 2-10% from 0.15 GeV to 0.5 GeV [14]. For pions, the momentum resolution is about 12% and almost independent of momentum. The azimuthal- and polar-angle resolution is about 4 mrad and 10 mrad respectively for pions and for protons with momenta larger than 0.5 GeV, deteriorating for lower proton momenta because of multiple scattering.

For each reconstructed track, the energy deposited along the particles' trajectory through the active detector components is used to determine the particle type. As protons and pions dominate the event sample, only the separation of these two particle types is considered. For each detection layer i, a particle-identification discriminator rdPID_i, which depends on the reconstructed three-momentum $|\vec{p}|$ and on the energy deposition dE

JHEP01(2014)077

normalized to pathlength, is calculated according to

$$\mathrm{rdPID}_i(dE;|\vec{p}|) = \log_{10}\frac{D_i\left(dE;\beta\gamma=\frac{|\vec{p}|}{M_p}\right)}{D_i\left(dE;\beta\gamma=\frac{|\vec{p}|}{M_\pi}\right)}, \tag{2.1}$$

where the "parent distributions" D_i are energy-deposition distributions normalized to unity, β is the ratio of the particle velocity to the speed of light, γ is the Lorentz factor, and M_p (M_π) is the proton (pion) mass. The combined particle-identification discriminator rdPID is the sum of the discriminators rdPID_i from the individual layers. A constraint on rdPID is chosen to distinguish between charged pions and protons, while providing an appropriate compromise between efficiency and contamination [21].

Details of the tracking, momentum reconstruction, and particle-identification procedures as well as detector performance studies are presented in ref. [14].

3 Event selection

A positron trigger is formed from a coincidence between three scintillator hodoscope planes and a lead-glass calorimeter. Following the approach of ref. [22], inclusive $ep \to eX$ events in the Deep-Inelastic Scattering (DIS) regime are selected by imposing the following kinematic requirements on the identified positron with the largest momentum in the event: $Q^2 > 1\,\mathrm{GeV}^2$, $W^2 > 9\,\mathrm{GeV}^2$, and $\nu < 22\,\mathrm{GeV}$, where W is the invariant mass of the $\gamma^* p$ system and $\nu \equiv (pq)/M_p$ the energy of the virtual photon in the target-rest frame. This sample of inclusive DIS events is employed for the determination of relative luminosities of the two beam-helicity states as inclusive DIS with virtual-photon exchange from unpolarized targets is invariant under reversal of the beam helicity.

Exclusive $ep \to e\gamma\pi N$ event candidates are selected from the DIS sample by requiring in the forward spectrometer the detection of exactly one identified positron in the absence of other charged particles and of exactly one signal cluster in the calorimeter not associated with the positron and hence signifying a real photon. The kinematic requirements on the identified positron and the photon cluster applied in ref. [12] are adjusted for this analysis as follows in order to optimize the selection of $ep \to e\gamma\pi N$ events. The cluster is required to represent an energy deposition above 8 GeV in the calorimeter and above 1 MeV in the preshower detector. Two kinematic constraints are applied: the polar angle $\theta_{\gamma^*\gamma}$ between the laboratory three-momenta of the virtual and real photons is limited to be less than 70 mrad, and the value of $-t$ is limited to be less than $1.2\,\mathrm{GeV}^2$. Here, $-t$ is calculated without the use of either the photon-energy measurement or recoil-detector information, under the hypothesis of an exclusive $ep \to e\gamma\Delta^+$ event. (The width of the Δ^+ is small compared to the experimental resolution.)

All recoil tracks identified as protons and positively charged pions are considered in order to select the associated reactions $ep \to e\gamma\pi^0 p$ and $ep \to e\gamma\pi^+ n$ in the Δ-resonance region. Kinematic event fitting is performed under the corresponding hypotheses using the three-momenta of the positron and photon measured in the forward spectrometer and

JHEP01(2014)077

the proton (pion) track in the recoil detector. The neutral pion (neutron) is not identified, therefore the fit enforces two four-momentum conservation equations based on the assumption of the $ep \to e\gamma\Delta^+$ reaction with Δ^+ decay to $p\pi^0(n\pi^+)$ assuming the PDG value of the $\Delta^+(1232)$ mass. In addition, adopting π^+ as proton candidates, the kinematic fit described in ref. [12] is performed in order to suppress $ep \to e\gamma p$ background events. The following constraints on the χ^2 of kinematic event fitting and on the rdPID values are optimized and applied for the selection of events from the associated channels:

- $ep \to e\gamma\pi^0 p$: $\chi^2_{ep\to e\gamma\pi^0 p} < 4.6$, $\chi^2_{ep\to e\gamma p} > 50$, and rdPID > 0 (to select protons),
- $ep \to e\gamma\pi^+ n$: $\chi^2_{ep\to e\gamma\pi^+ n} < 4.6$, $\chi^2_{ep\to e\gamma p} > 50$, and rdPID < 0 (to select pions).

Kinematic distributions obtained from experimental data are compared with a mixture of simulated data samples. Following the approach of refs. [12, 23, 24], BH events are simulated using the Mo-Tsai formalism [25], by an event generator based on ref. [26] and described in detail in ref. [27]. This sample of BH events includes events from associated production generated using the parametrization of the form factor for the resonance region from ref. [28]. The individual cross sections for single-meson decay channels of Δ^+ are treated according to the MAID2000 model [29]. (Neither the DVCS process nor the associated DVCS process are included in the simulation since for the latter an event generator is unavailable.) Semi-Inclusive DIS (SIDIS) events are simulated using an event generator based on LEPTO [30] with a set of JETSET [31] fragmentation parameters tuned for HERMES kinematic conditions [32], including the RADGEN [33] package for radiative effects.

The χ^2 distributions from kinematic fitting under the hypothesis of the associated reaction obtained for experimental and simulated data are compared in figure 1 for the channels $ep \to e\gamma\pi^0 p$ (left panel) and $ep \to e\gamma\pi^+ n$ (right panel). For both channels, acceptable agreement in the shape of the distributions is observed, given that the Monte Carlo event generator does not include the DVCS processes.

In figure 2 comparisons of distributions over the kinematic variables $-t$, x_B, and Q^2 are shown for the associated channels $ep \to e\gamma\pi^0 p$ (left panel) and $ep \to e\gamma\pi^+ n$ (right panel). This comparison provides evidence that the Monte Carlo description of the associated BH reaction used in previous analyses [12, 22–24, 34] accounts for most of the observed yields.

The fractional contributions from the associated reaction, $ep \to e\gamma p$, and SIDIS processes, obtained by analyzing Monte Carlo data in the same way as described above, are listed with their statistical uncertainties in table 1 for the channel $ep \to e\gamma\pi^0 p$ and in table 2 for the channel $ep \to e\gamma\pi^+ n$ in one kinematic bin covering the entire kinematic region considered here ("overall") and in kinematic bins of $-t$, x_B, and Q^2.

4 Extraction of asymmetry amplitudes

Fourier amplitudes of the single-charge beam-helicity asymmetry $\mathcal{A}_{\mathrm{LU}}(\phi; e_\ell)$ are extracted in a manner similar to that applied in ref. [34]. The extraction is based on an extended maximum-likelihood fit [35], unbinned in the azimuthal angle ϕ.

JHEP01(2014)077

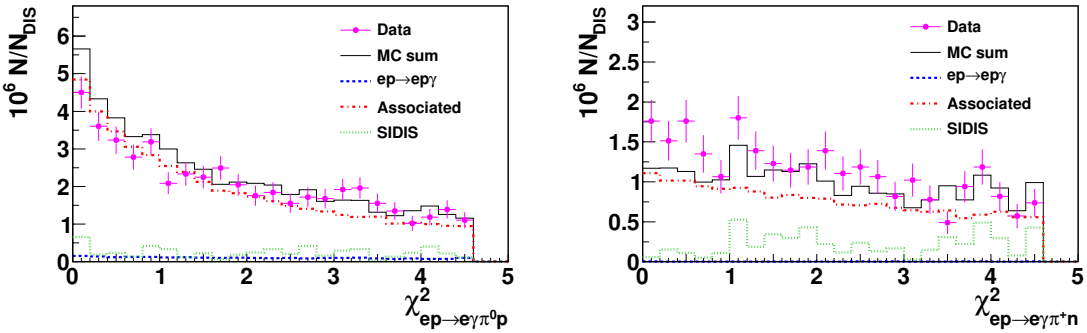

Figure 1. Distributions of $\chi^2_{ep\to e\gamma\pi^0 p}$ (left) and $\chi^2_{ep\to e\gamma\pi^+ n}$ (right) for the channel $ep \to e\gamma\pi^0 p$ and $ep \to e\gamma\pi^+ n$, respectively. Experimental data are presented by points, and the results of the Monte Carlo simulation by lines. Contributions from the associated, $ep \to e\gamma p$, and SIDIS reactions are shown by red dash-dotted, blue dashed, and green dotted lines, respectively (color online). Data and Monte Carlo yields are normalized to the corresponding numbers of DIS events.

Kinematic bin		$ep \to e\gamma\pi^0 p$ [%]	$ep \to e\gamma p$ [%]	SIDIS [%]
Overall		85 ± 1	4.6 ± 0.1	11 ± 1
$-t$ [GeV^2]	<0.17	79 ± 2	13.5 ± 0.5	8 ± 3
	0.17-0.30	86 ± 3	3.9 ± 0.2	11 ± 3
	0.30-0.50	86 ± 2	2.1 ± 0.1	12 ± 2
	0.50-1.20	86 ± 2	1.3 ± 0.1	13 ± 2
x_B	0.03-0.07	86 ± 2	6.3 ± 0.3	8 ± 2
	0.07-0.10	84 ± 3	5.1 ± 0.2	11 ± 3
	0.10-0.15	88 ± 2	3.5 ± 0.2	9 ± 2
	0.15-0.35	79 ± 2	3.1 ± 0.2	18 ± 2
Q^2 [GeV^2]	1.00-1.50	78 ± 3	6.3 ± 0.4	16 ± 4
	1.50-2.30	86 ± 2	5.5 ± 0.2	8 ± 2
	2.30-3.50	86 ± 2	3.9 ± 0.2	10 ± 2
	3.50-10.0	86 ± 2	3.1 ± 0.2	11 ± 2

Table 1. Monte-Carlo-estimated fractional contributions to the measured yields by $ep \to e\gamma\pi^0 p$, $ep \to e\gamma p$, and SIDIS reactions in the selected sample of $ep \to e\gamma\pi^0 p$ events.

The distribution of the expectation value of the yield for scattering of a longitudinally polarized positron beam with polarization P_ℓ from an unpolarized hydrogen target is given by

$$\langle \mathcal{N} \rangle(\phi; e_\ell, P_\ell) = \mathcal{L}(e_\ell, P_\ell)\eta(\phi)\sigma_{\rm UU}(\phi)\left[1 + P_\ell \mathcal{A}_{\rm LU}(\phi; e_\ell)\right], \tag{4.1}$$

where $\mathcal{L}$ denotes the integrated luminosity determined by counting inclusive DIS events and η the detection efficiency. The asymmetry $\mathcal{A}_{\rm LU}(\phi; e_\ell)$ is expanded in terms of harmonics in ϕ in order to extract azimuthal asymmetry amplitudes:

$$\mathcal{A}_{\rm LU}(\phi; e_\ell) \simeq A_{\rm LU}^{\sin\phi} \sin\phi + A_{\rm LU}^{\sin(2\phi)} \sin(2\phi), \tag{4.2}$$

where the approximation is due to the truncation of the infinite Fourier series.

As a test of the normalization of the fit, the maximum-likelihood fit is repeated including the term $A_{\rm LU}^{\cos(0\phi)}$. This term is found to be compatible with zero within statistical uncertainties and to have negligible impact on the resulting asymmetry amplitudes.

JHEP01(2014)077

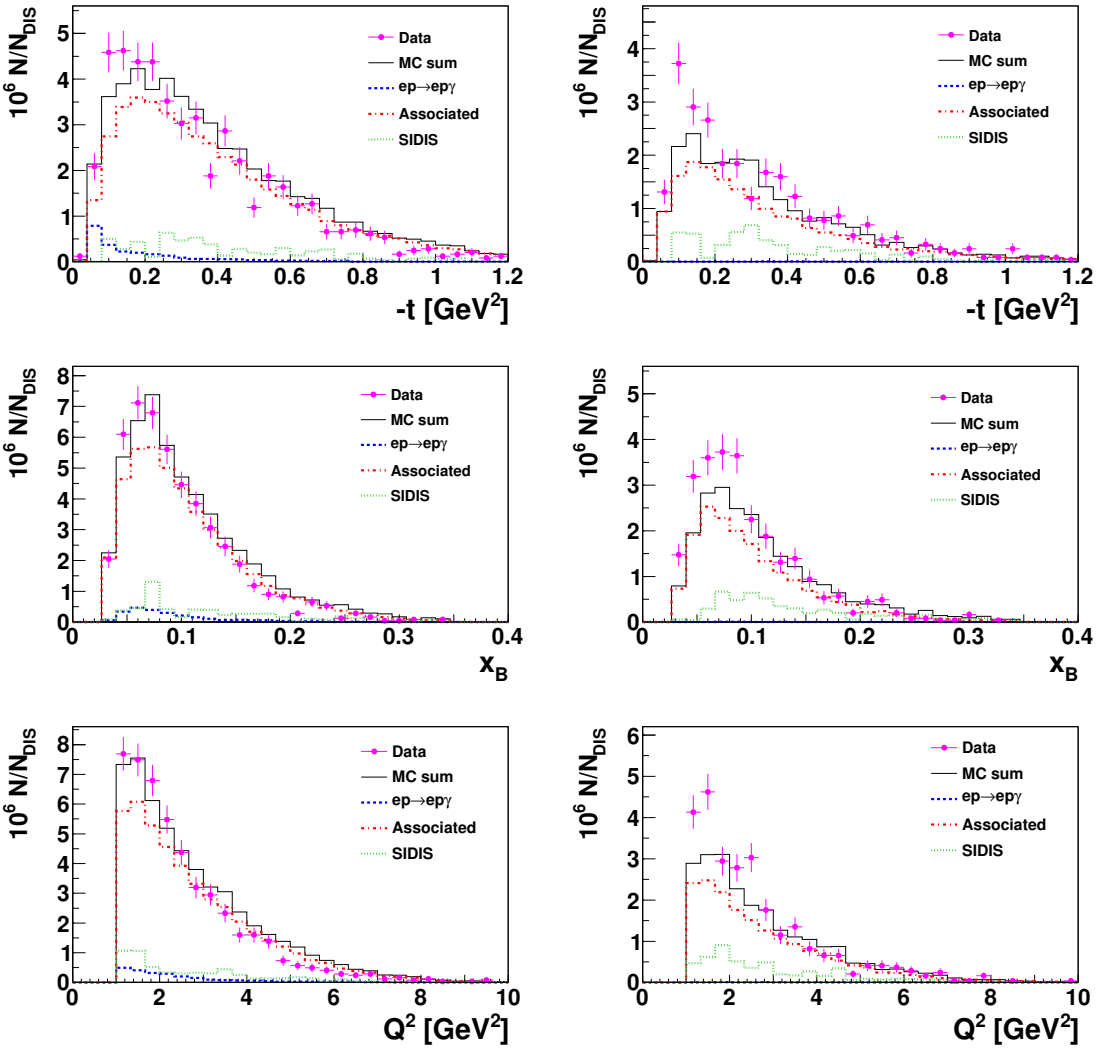

Figure 2. Distributions of t (top row), x_B (middle row), and Q^2 (bottom row) for the associated channel $ep \to e\gamma\pi^0 p$ (left column) and $ep \to e\gamma\pi^+ n$ (right column). Notations are the same as in figure 1.

5 Background corrections and systematic uncertainties

The Monte Carlo simulation shows that the selected samples of associated events contain contributions from two different sources of background. The most significant contribution originates from SIDIS production of neutral pions from the fragmenting struck quark, $ep \to e\pi^0 X$, with the hadronic system X containing a pion or proton in the recoil detector. According to the Monte Carlo simulation, its contribution varies from 8% to 18% in the case of the channel $ep \to e\gamma\pi^0 p$ and from 10% to 36% in the case of the channel $ep \to e\gamma\pi^+ n$, depending on the kinematic bin (see tables 1 and 2). The second source of background is the $ep \to e\gamma p$ reaction, contributing from 1% to 14% for the channel $ep \to e\gamma\pi^0 p$ and negligibly for the channel $ep \to e\gamma\pi^+ n$.

JHEP01(2014)077

Kinematic bin		$ep \to e\gamma\pi^+n$ [%]	$ep \to e\gamma p$ [%]	SIDIS [%]
Overall		77 ± 2	0.2 ± 0.1	23 ± 3
$-t$ [GeV^2]	<0.17	82 ± 5	0.1 ± 0.1	18 ± 5
	0.17-0.30	80 ± 5	0.2 ± 0.1	20 ± 5
	0.30-0.50	74 ± 4	0.3 ± 0.1	26 ± 5
	0.50-1.20	72 ± 4	0.3 ± 0.2	28 ± 5
x_B	0.03-0.07	90 ± 4	0.2 ± 0.3	10 ± 4
	0.07-0.10	77 ± 5	0.3 ± 0.1	23 ± 6
	0.10-0.15	74 ± 4	0.2 ± 0.1	26 ± 6
	0.15-0.35	64 ± 4	0.2 ± 0.1	36 ± 5
Q^2 [GeV^2]	1.00-1.50	82 ± 6	0.2 ± 0.1	18 ± 7
	1.50-2.30	74 ± 4	0.2 ± 0.1	26 ± 6
	2.30-3.50	80 ± 4	0.3 ± 0.1	20 ± 5
	3.50-10.0	75 ± 3	0.2 ± 0.1	25 ± 3

Table 2. Monte-Carlo-estimated fractional contributions to the measured yields by $ep \to e\gamma\pi^+n$, $ep \to e\gamma p$, and SIDIS reactions in the selected sample of $ep \to e\gamma\pi^+n$ events.

The asymmetry amplitudes $A_{\rm SIDIS}$ are extracted from experimental data using information from only the forward spectrometer. This approach is based on the assumption that the asymmetry for SIDIS π^0 production is little affected by the requirement of the detection in the recoil detector of either a proton or a π^+ satisfying the kinematic fit for the associated reaction. Monte Carlo studies showed [36] that the asymmetry extracted for SIDIS π^0 production is insensitive to event selection using one or two photons. Thus, in order to estimate the asymmetry of semi-inclusive π^0 background from data, a "two-photon analysis" is performed. Instead of requiring one trackless cluster in the calorimeter, two trackless clusters are selected with the energy deposition in the preshower detector larger than 1 MeV. In addition, the energy of the leading photon is required to be larger than 8 GeV and the energy of the non-leading one to be above 1 GeV. The beam-helicity asymmetry amplitudes are extracted with the same maximum-likelihood fit method as for the associated sample and are found to be consistent with zero. These asymmetry amplitudes are used to correct for the contribution from the SIDIS reaction in both the $ep \to e\gamma\pi^0p$ and $ep \to e\gamma\pi^+n$ channels. In order to correct for the small contribution from $ep \to e\gamma p$, its beam-helicity asymmetry amplitude $A_{e\gamma p}$ measured with kinematically complete event reconstruction [12] is used. The slightly different kinematic constraints applied there are not expected to significantly affect this small correction.

The measured asymmetry amplitudes $A_{\rm meas.}$ are corrected for the above mentioned sources of background according to:

$$A_{\rm corr.} = \frac{A_{\rm meas.} - f_{e\gamma p}A_{e\gamma p} - f_{\rm SIDIS}A_{\rm SIDIS}}{1 - f_{e\gamma p} - f_{\rm SIDIS}}, \tag{5.1}$$

where $f_{e\gamma p}$ and $f_{\rm SIDIS}$ are the simulated fractional contributions to the yield from the $ep \to e\gamma p$ and SIDIS reactions and $A_{e\gamma p}$ and $A_{\rm SIDIS}$ the corresponding measured asymmetry amplitudes. The magnitude of the difference between corrected and measured amplitudes is assigned as systematic uncertainty (see tables 3 and 4). This approach takes into account

JHEP01(2014)077

the observed differences between data and Monte Carlo simulations presented in figures 1 and 2.

In addition to systematic uncertainties due to the background correction described above, the remaining sources of systematic uncertainties on the extracted asymmetry amplitudes arise from the spectrometer and recoil-detector acceptance, smearing, and finite bin width. In order to estimate the combined contribution to the systematic uncertainty from these three sources, the so-called "all-in-one" method is used, which was first employed in the analysis described in ref. [34] and was also used by the latest DVCS analyses [12, 23, 24]. Due to the lack of knowledge about the associated DVCS process, there is no applicable (GPD) model for use in the Monte Carlo generator, leaving only the BH process with no interference to produce a beam-helicity asymmetry. For an estimate of the above mentioned systematic effects, an artificial t-dependent asymmetry of the expected asymptotic form $A(-t) = C\sqrt{-t}\sin(\phi) + 0\sin(2\phi)$ is implemented for the associated BH process. The following values of the constant parameter C are applied on generator level: $C = \{-0.4, -0.2, 0.1, 0.3, 0.5\}$. (None of these values are conclusively excluded by the experimental data). The Monte Carlo samples are generated for each beam-polarization state separately, passed through a detailed GEANT [37] simulation of the HERMES forward spectrometer and recoil detector, and reconstructed with the same reconstruction and analysis algorithms as for real data. After selection of the associated Monte Carlo sample, the maximum-likelihood fit is performed to extract asymmetry amplitudes in each kinematic bin, referred to as reconstructed asymmetry amplitudes. The estimate of the systematic uncertainty due to acceptance, smearing, and finite bin width is obtained as the difference between the reconstructed Monte Carlo asymmetry amplitudes and those calculated at the reconstructed mean values of $-t$, x_B, and Q^2 in each kinematic bin. The procedure is repeated for each implemented asymmetry separately for both associated channels. The all-in-one systematic uncertainties are taken as the root mean square of the differences between reconstructed and calculated asymmetry amplitudes for all parameter values of the implemented asymmetry, and are presented in tables 3 and 4.

The impact of trigger inefficiency is studied and found to be negligible.

The resulting systematic uncertainties are calculated as the quadratic sum of systematic uncertainties from background correction and all-in-one estimates of acceptance, smearing, and finite bin width effects. They are summarized in tables 3 and 4 for each kinematic bin for the channels $ep \to e\gamma\pi^0 p$ and $ep \to e\gamma\pi^+ n$, respectively.

6 Results and discussion

Results on asymmetry amplitudes corrected for background contributions are presented in figures 3 and 4, and in tables 5 and 6. Each of the asymmetry amplitudes is shown extracted in one bin covering the entire kinematic region ("overall") and also projected against $-t$, x_B, and Q^2. The beam-helicity asymmetry amplitudes are subject to an additional scale uncertainty of 1.96% due to the measurement of the beam polarization. All asymmetry amplitudes are found to be consistent with zero within large experimental uncertainties.

JHEP01(2014)077

		$\delta_{\rm syst} A_{LU}^{\sin\phi}$ $(ep \to e\gamma\pi^0 p)$			$\delta_{\rm syst} A_{LU}^{\sin(2\phi)}$ $(ep \to e\gamma\pi^0 p)$		
Kinematic bin		Bg. corr.	All-in-one	Total	Bg. corr.	All-in-one	Total
Overall		(−) 0.013	0.008	0.016	(−) 0.009	0.004	0.010
$-t$ [GeV^2]	<0.17	(−) 0.049	0.015	0.051	(−) 0.004	0.007	0.009
	0.17-0.30	(+) 0.049	0.008	0.050	(+) 0.031	0.005	0.031
	0.30-0.50	(−) 0.027	0.017	0.032	(−) 0.013	0.001	0.013
	0.50-1.20	(−) 0.043	0.011	0.044	(−) 0.059	0.005	0.059
x_B	0.03-0.07	(+) 0.013	0.015	0.020	(−) 0.026	0.009	0.027
	0.07-0.10	(−) 0.029	0.001	0.029	(−) 0.019	0.008	0.021
	0.10-0.15	(−) 0.013	0.006	0.014	(+) 0.022	0.012	0.025
	0.15-0.35	(−) 0.144	0.021	0.146	(+) 0.097	0.013	0.098
Q^2 [GeV^2]	1.00-1.50	(+) 0.006	0.005	0.008	(+) 0.042	0.009	0.043
	1.50-2.30	(+) 0.032	0.019	0.037	(−) 0.059	0.009	0.060
	2.30-3.50	(−) 0.033	0.010	0.035	(+) 0.017	0.009	0.019
	3.50-10.0	(−) 0.063	0.012	0.065	(+) 0.040	0.010	0.041

Table 3. Individual contributions to the total systematic uncertainties from background correction and all-in-one estimates of acceptance, smearing, and finite bin width effects for the channel $ep \to e\gamma\pi^0 p$. The sign of the background corrections is shown in parentheses.

		$\delta_{\rm syst} A_{LU}^{\sin\phi}$ $(ep \to e\gamma\pi^+ n)$			$\delta_{\rm syst} A_{LU}^{\sin(2\phi)}$ $(ep \to e\gamma\pi^+ n)$		
Kinematic bin		Bg. corr.	All-in-one	Total	Bg. corr.	All-in-one	Total
Overall		(−) 0.005	0.010	0.012	(−) 0.027	0.011	0.029
$-t$ [GeV^2]	<0.17	(−) 0.010	0.001	0.010	(−) 0.186	0.023	0.187
	0.17-0.30	(+) 0.044	0.016	0.047	(+) 0.053	0.009	0.054
	0.30-0.50	(−) 0.042	0.017	0.045	(+) 0.002	0.004	0.005
	0.50-1.20	(+) 0.001	0.012	0.012	(−) 0.001	0.015	0.015
x_B	0.03-0.07	(−) 0.003	0.010	0.011	(−) 0.040	0.018	0.044
	0.07-0.10	(−) 0.056	0.035	0.066	(−) 0.023	0.012	0.025
	0.10-0.15	(+) 0.019	0.012	0.022	(+) 0.013	0.009	0.016
	0.15-0.35	(+) 0.025	0.022	0.034	(−) 0.147	0.019	0.148
Q^2 [GeV^2]	1.00-1.50	(−) 0.078	0.014	0.079	(−) 0.027	0.020	0.034
	1.50-2.30	(−) 0.014	0.004	0.015	(−) 0.078	0.004	0.079
	2.30-3.50	(−) 0.009	0.024	0.026	(−) 0.016	0.010	0.019
	3.50-10.0	(+) 0.049	0.013	0.051	(+) 0.011	0.023	0.025

Table 4. Individual contributions to the total systematic uncertainties from background correction and all-in-one estimates of acceptance, smearing, and finite bin width effects for the channel $ep \to e\gamma\pi^+ n$. The sign of the background corrections is shown in parentheses.

The model of ref. [7] described in section 1, employing the VGG model [8, 38] for the nucleon GPDs, predicts the $\sin\phi$ asymmetry amplitudes to be about -0.15 in the case of the $ep \to e\gamma\pi^0 p$ channel and about -0.10 in the case of the $ep \to e\gamma\pi^+ n$ channel.[1] The presented experimental results do not exclude this model.

Recently, HERMES published results on the single-charge beam-helicity asymmetry arising from DVCS with kinematically complete event reconstruction [12]. The main result of this publication was that after removal of associated background from the data sample the magnitude of the leading asymmetry amplitude increased. This increase is consistent

[1] In ref. [7], a different convention for the ϕ angle definition was used leading to the opposite sign of asymmetry amplitudes.

JHEP01(2014)077

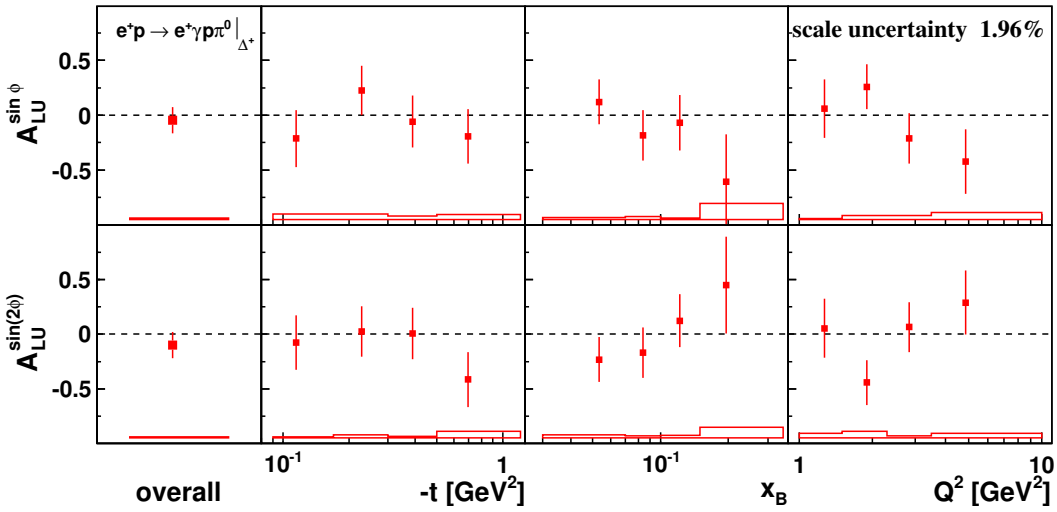

Figure 3. Amplitudes of the single-charge beam-helicity asymmetry extracted in the associated channel $ep \to e\gamma\pi^0 p$ obtained with recoil-proton reconstruction. The amplitudes are presented in projections of $-t$, x_{B}, and Q^2. The "overall" results shown in the very left panel are extracted in a single kinematic bin covering the entire kinematic acceptance. Statistical (systematic) uncertainties are represented by error bars (bands). A separate scale uncertainty arising from the measurement of the beam polarization amounts to 1.96%.

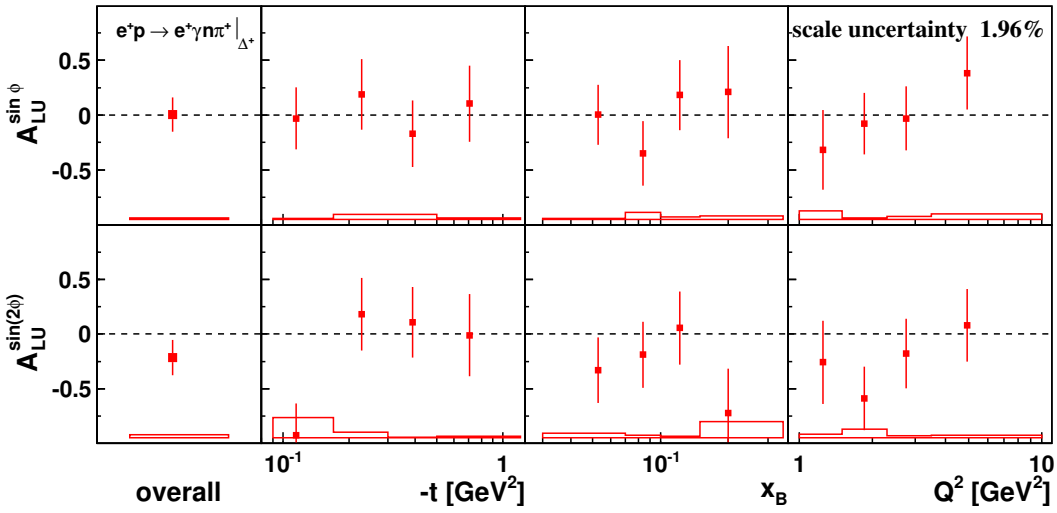

Figure 4. Amplitudes of the single-charge beam-helicity asymmetry extracted in the associated channel $ep \to e\gamma\pi^+ n$ obtained with recoil-pion reconstruction. Otherwise as for figure 3.

with the small magnitude of the asymmetries in the two associated channels obtained in this analysis. Effectively, the background from the associated reaction acts as a dilution in the beam-helicity asymmetries measured previously by HERMES using the missing-mass technique [23, 24].

JHEP01(2014)077

Kinematic bin		Number of events	$\langle -t \rangle$ [GeV^2]	$\langle x_B \rangle$	$\langle Q^2 \rangle$ [GeV^2]	$A_{LU}^{\sin\phi}$ $\pm\delta_{\text{stat}} \pm \delta_{\text{syst}}$	$A_{LU}^{\sin(2\phi)}$ $\pm\delta_{\text{stat}} \pm \delta_{\text{syst}}$
Overall		1185	0.35	0.10	2.54	$-0.05 \pm 0.12 \pm 0.02$	$-0.10 \pm 0.12 \pm 0.01$
$-t$[GeV^2]	0.00-0.17	305	0.12	0.07	1.84	$-0.21 \pm 0.26 \pm 0.05$	$-0.08 \pm 0.25 \pm 0.01$
	0.17-0.30	303	0.23	0.09	2.38	$0.23 \pm 0.22 \pm 0.05$	$0.03 \pm 0.23 \pm 0.03$
	0.30-0.50	304	0.39	0.11	2.74	$-0.06 \pm 0.24 \pm 0.03$	$0.01 \pm 0.25 \pm 0.01$
	0.50-1.20	273	0.69	0.12	3.27	$-0.49 \pm 0.30 \pm 0.04$	$-0.55 \pm 0.33 \pm 0.06$
x_B	0.03-0.07	417	0.30	0.05	1.49	$0.12 \pm 0.20 \pm 0.02$	$-0.23 \pm 0.21 \pm 0.03$
	0.07-0.10	318	0.28	0.08	2.16	$-0.18 \pm 0.23 \pm 0.03$	$-0.17 \pm 0.23 \pm 0.02$
	0.10-0.15	290	0.39	0.12	3.11	$-0.07 \pm 0.25 \pm 0.01$	$0.12 \pm 0.24 \pm 0.03$
	0.15-0.35	160	0.54	0.20	4.99	$-0.61 \pm 0.43 \pm 0.15$	$0.45 \pm 0.44 \pm 0.10$
Q^2[GeV^2]	1.00-1.50	294	0.26	0.05	1.27	$0.06 \pm 0.27 \pm 0.01$	$0.05 \pm 0.27 \pm 0.04$
	1.50-2.30	364	0.31	0.08	1.89	$0.26 \pm 0.20 \pm 0.04$	$-0.44 \pm 0.20 \pm 0.06$
	2.30-3.50	304	0.38	0.11	2.84	$-0.21 \pm 0.23 \pm 0.04$	$0.07 \pm 0.23 \pm 0.02$
	3.50-10.0	223	0.49	0.17	4.85	$-0.42 \pm 0.30 \pm 0.07$	$0.29 \pm 0.29 \pm 0.04$

Table 5. Results on amplitudes extracted in the associated channel $ep \to e\gamma\pi^0 p$.

Kinematic bin		Number of events	$\langle -t \rangle$ [GeV^2]	$\langle x_B \rangle$	$\langle Q^2 \rangle$ [GeV^2]	$A_{LU}^{\sin\phi}$ $\pm\delta_{\text{stat}} \pm \delta_{\text{syst}}$	$A_{LU}^{\sin(2\phi)}$ $\pm\delta_{\text{stat}} \pm \delta_{\text{syst}}$
Overall		653	0.32	0.10	2.57	$0.01 \pm 0.15 \pm 0.01$	$-0.21 \pm 0.16 \pm 0.03$
$-t$[GeV^2]	0.00-0.17	218	0.12	0.08	1.90	$-0.03 \pm 0.28 \pm 0.01$	$-0.93 \pm 0.29 \pm 0.19$
	0.17-0.30	154	0.23	0.10	2.49	$0.19 \pm 0.32 \pm 0.05$	$0.18 \pm 0.33 \pm 0.05$
	0.30-0.50	156	0.39	0.11	2.88	$-0.17 \pm 0.30 \pm 0.05$	$0.11 \pm 0.32 \pm 0.01$
	0.50-1.20	125	0.71	0.12	3.47	$0.11 \pm 0.35 \pm 0.01$	$-0.01 \pm 0.38 \pm 0.02$
x_B	0.03-0.07	228	0.28	0.05	1.48	$0.00 \pm 0.27 \pm 0.01$	$-0.33 \pm 0.30 \pm 0.04$
	0.07-0.10	183	0.28	0.08	2.20	$-0.35 \pm 0.29 \pm 0.07$	$-0.19 \pm 0.30 \pm 0.03$
	0.10-0.15	156	0.34	0.12	3.13	$0.18 \pm 0.32 \pm 0.02$	$0.06 \pm 0.33 \pm 0.02$
	0.15-0.35	86	0.49	0.20	5.26	$0.21 \pm 0.42 \pm 0.03$	$-0.72 \pm 0.41 \pm 0.15$
Q^2[GeV^2]	1.00-1.50	158	0.24	0.05	1.25	$-0.32 \pm 0.36 \pm 0.08$	$-0.26 \pm 0.38 \pm 0.03$
	1.50-2.30	189	0.26	0.08	1.85	$-0.08 \pm 0.28 \pm 0.02$	$-0.59 \pm 0.29 \pm 0.08$
	2.30-3.50	173	0.35	0.10	2.76	$-0.03 \pm 0.29 \pm 0.03$	$-0.18 \pm 0.32 \pm 0.02$
	3.50-10.0	133	0.47	0.17	4.93	$0.38 \pm 0.33 \pm 0.05$	$0.08 \pm 0.33 \pm 0.03$

Table 6. Results on amplitudes extracted in the associated channel $ep \to e\gamma\pi^+ n$.

7 Summary

Amplitudes of the beam-helicity asymmetry are measured at HERMES in exclusive associated production of real photons, $ep \to e\gamma\pi N$, by longitudinally polarized positrons incident on an unpolarized hydrogen target. The selected $ep \to e\gamma\pi^0 p$ ($ep \to e\gamma\pi^+ n$) event sample is estimated to contain on average 11% (23%) contribution from SIDIS production, which is corrected for in the analysis. Corrections for the small contributions from $ep \to e\gamma p$ are applied using asymmetry amplitudes obtained previously by HERMES. All asymmetry amplitudes are found to be consistent with zero within experimental uncertainties that are at best ± 0.12 in the full acceptance. The only available theoretical estimates [7] for the asymmetry amplitudes are consistent with the measurements. This finding may offer support for the model of transition GPDs in terms of nucleon GPDs, based on the soft-pion technique and the large N_c limit.

JHEP01(2014)077

Acknowledgments

We gratefully acknowledge the DESY management for its support and the staff at DESY and the collaborating institutions for their significant effort. This work was supported by the Ministry of Economy and the Ministry of Education and Science of Armenia; the FWO-Flanders and IWT, Belgium; the Natural Sciences and Engineering Research Council of Canada; the National Natural Science Foundation of China; the Alexander von Humboldt Stiftung, the German Bundesministerium für Bildung und Forschung (BMBF), and the Deutsche Forschungsgemeinschaft (DFG); the Italian Istituto Nazionale di Fisica Nucleare (INFN); the MEXT, JSPS, and G-COE of Japan; the Dutch Foundation for Fundamenteel Onderzoek der Materie (FOM); the Russian Academy of Science and the Russian Federal Agency for Science and Innovations; the Basque Foundation for Science (IKERBASQUE) and the UPV/EHU under program UFI 11/55; the U.K. Engineering and Physical Sciences Research Council, the Science and Technology Facilities Council, and the Scottish Universities Physics Alliance; the U.S. Department of Energy (DOE) and the National Science Foundation (NSF); as well as the European Community Research Infrastructure Integrating Activity under the FP7 "Study of strongly interacting matter (HadronPhysics3, Grant Agreement number 283286)".

References

[1] D. Müller, D. Robaschik, B. Geyer, F.-M. Dittes and J. Hořejši, *Wave functions, evolution equations and evolution kernels from light ray operators of QCD*, *Fortsch. Phys.* **42** (1994) 101 [hep-ph/9812448] [INSPIRE].

[2] A.V. Radyushkin, *Scaling limit of deeply virtual Compton scattering*, *Phys. Lett.* **B 380** (1996) 417 [hep-ph/9604317] [INSPIRE].

[3] X. Ji, *Deeply virtual Compton scattering*, *Phys. Rev.* **D 55** (1997) 7114 [hep-ph/9609381] [INSPIRE].

[4] X. Ji, *Gauge-Invariant Decomposition of Nucleon Spin*, *Phys. Rev. Lett.* **78** (1997) 610 [hep-ph/9603249] [INSPIRE].

[5] M. Burkardt, *Impact parameter dependent parton distributions and off forward parton distributions for $\zeta \to 0$*, *Phys. Rev.* **D 62** (2000) 071503(R) [*Erratum ibid.* **D 66** (2002) 119903] [hep-ph/0005108] [INSPIRE].

[6] L.L Frankfurt, M.V. Polyakov, M. Strikman and M. Vanderhaeghen, *Hard Exclusive Electroproduction of Decuplet Baryons in the Large-N_c Limit*, *Phys. Rev. Lett.* **84** (2000) 2589 [hep-ph/9911381] [INSPIRE].

[7] P.A.M. Guichon, L. Mossé and M. Vanderhaeghen, *Pion production in deeply virtual Compton scattering*, *Phys. Rev.* **D 68** (2003) 034018 [hep-ph/0305231] [INSPIRE].

[8] K. Goeke, M.V. Polyakov and M. Vanderhaeghen, *Hard exclusive reactions and the structure of hadrons*, *Prog. Part. Nucl. Phys.* **47** (2001) 401 [hep-ph/0106012] [INSPIRE].

JHEP01(2014)077

[9] D.A. McPherson, D.C. Gates, R.W. Kenney and W.P. Swanson, *Positive Photopion Production from Hydrogen Near Threshold*, *Phys. Rev.* **136** (1964) B1465.

[10] M. MacCormick, G. Audit, N. d'Hose, L. Ghedira, V. Isbert et al., *Total photoabsorption cross-sections for ^1H, ^2H, and ^3He from 200 MeV to 800 MeV*, *Phys. Rev.* **C 53** (1996) 41 [INSPIRE].

[11] GDH and A2 collaboration, J. Ahrens et al., *Helicity Dependence of $\gamma p \to N\pi$ below 450 MeV and Contribution to the Gerasimov-Drell-Hearn Sum Rule*, *Phys. Rev. Lett.* **84** (2000) 5950 [INSPIRE].

[12] HERMES collaboration, A. Airapetian et al., *Beam-helicity asymmetry arising from deeply virtual Compton scattering measured with kinematically complete event reconstruction*, *JHEP* **10** (2012) 042 [arXiv:1206.5683] [INSPIRE].

[13] A. Bacchetta, U. D'Alesio, M. Diehl and C.A. Miller, *Single-spin asymmetries: The Trento conventions*, *Phys. Rev.* **D 70** (2004) 117504 [hep-ph/0410050] [INSPIRE].

[14] A. Airapetian, E. Aschenauer, S. Belostotski, A. Borissov, A. Borisenko et al., *The HERMES recoil detector*, 2013 *JINST* **8** P05012 [arXiv:1302.6092] [INSPIRE].

[15] HERMES collaboration, K. Ackerstaff et al., *The HERMES Spectrometer*, *Nucl. Instrum. Meth.* **A 417** (1998) 230 [hep-ex/9806008] [INSPIRE].

[16] A. Sokolov and I. Ternov, *On Polarization and spin effects in the theory of synchrotron radiation*, *Sov. Phys. Dokl.* **8** (1964) 1203 [INSPIRE].

[17] J. Buon and K. Steffen, *HERA variable-energy "mini" spin rotator and head-on ep collision scheme with choice of electron helicity*, *Nucl. Instrum. Meth.* **A 245** (1986) 248 [INSPIRE].

[18] M. Beckmann, A. Borissov, S. Brauksiepe, F. Burkart, H. Fischer et al., *The Longitudinal Polarimeter at HERA*, *Nucl. Instrum. Meth.* **A 479** (2002) 334 [physics/0009047] [INSPIRE].

[19] D.P. Barber, M. Böge, H. Böttcher, H.-D. Bremer, R. Brinkmann et al. *High spin polarization at the HERA electron storage ring*, *Nucl. Instrum. Meth.* **A 338** (1994) 166 [INSPIRE].

[20] B. Sobloher, R. Fabbri, T. Behnke, J. Olsson, D. Pitzl et al., *Polarisation at HERA - Reanalysis of the HERA II Polarimeter Data*, *DESY Report* 11-259 [arXiv:1201.2894] [INSPIRE].

[21] X. Lu, *The HERMES Recoil Detector: Particle Identification and Determination of Detector Efficiency of the Scintillating Fiber Tracker*, Master Thesis, Universität Hamburg, Germany, DESY-THESIS-2009-043 (2009) [INSPIRE].

[22] HERMES collaboration, A. Airapetian et al., *Beam-charge azimuthal asymmetry and deeply virtual compton scattering*, *Phys. Rev.* **D 75** (2007) 011103(R) [hep-ex/0605108] [INSPIRE].

[23] HERMES collaboration, A. Airapetian et al., *Separation of contributions from deeply virtual Compton scattering and its interference with the Bethe-Heitler process in measurements on a hydrogen target*, *JHEP* **11** (2009) 083 [arXiv:0909.3587] [INSPIRE].

[24] HERMES collaboration, A. Airapetian et al., *Beam-helicity and beam-charge asymmetries associated with deeply virtual Compton scattering on the unpolarised proton*, *JHEP* **07** (2012) 032 [arXiv:1203.6287] [INSPIRE].

[25] L.W. Mo and Y.S. Tsai, *Radiative Corrections to Elastic and Inelastic ep and μp Scattering*, *Rev. Mod. Phys.* **41** (1969) 205 [INSPIRE].

JHEP01(2014)077

[26] V.A. Korotkov and W.-D. Nowak, *Future measurements of deeply virtual Compton scattering*, *Eur. Phys. J.* **C 23** (2002) 455 [hep-ph/0108077] [INSPIRE].

[27] B. Krauß, *Deeply Virtual Compton Scattering and the HERMES-Recoil-Detector*, Ph.D. Thesis, Friedrich-Alexander Universität Erlangen-Nürnberg, Germany, DESY-THESIS-2005-008 (2005) [INSPIRE].

[28] F.W. Brasse, W. Flauger, J. Gayler, S.P. Goel, R. Haidan et al., *Parametrization of the q^2 dependence of $\gamma_V p$ total cross sections in the resonance region*, *Nucl. Phys.* **B 110** (1976) 413 [INSPIRE].

[29] D. Drechsel, O. Hanstein, S.S. Kamalov and L. Tiator, *A Unitary isobar model for pion photoproduction and electroproduction on the proton up to 1 GeV*, *Nucl. Phys.* **A 645** (1999) 145 [nucl-th/9807001] [INSPIRE].

[30] G. Ingelman, A. Edin and J. Rathsman, *LEPTO 6.5: A Monte Carlo generator for deep inelastic lepton-nucleon scattering*, *Comput. Phys. Commun.* **101** (1997) 108 [hep-ph/9605286] [INSPIRE].

[31] T. Sjöstrand, *High-energy physics event generation with PYTHIA 5.7 and JETSET 7.4*, *Comput. Phys. Commun.* **82** (1994) 74 [INSPIRE].

[32] A. Hillenbrand, *Measurement and Simulation of the Fragmentation Process at HERMES*, Ph.D. Thesis, Friedrich-Alexander Universität Erlangen-Nürnberg, Germany, DESY-THESIS-2005-035 (2005) [INSPIRE].

[33] I. Akushevich, H. Böttcher and D. Ryckbosch, *RADGEN 1.0: Monte Carlo Generator for Radiative Events in DIS on Polarized and Unpolarized Targets*, hep-ph/9906408 [INSPIRE].

[34] HERMES collaboration, A. Airapetian et al., *Measurement of azimuthal asymmetries with respect to both beam charge and transverse target polarization in exclusive electroproduction of real photons*, *JHEP* **06** (2008) 066 [arXiv:0802.2499] [INSPIRE].

[35] R. Barlow, *Extended maximum likelihood*, *Nucl. Instrum. Meth.* **A 297** (1990) 496 [INSPIRE].

[36] Z. Ye, *Transverse Target-Spin Asymmetry Associated with Deeply Virtual Compton Scattering on the Proton and A Resulting Model-Dependent Constraint on the Total Angular Momentum of Quarks in the Nucleon*, Ph.D. Thesis, Universität Hamburg, Germany, DESY-THESIS-2007-005 (2006) [INSPIRE].

[37] R. Brun, R. Hagelberg, M. Hansroul and J. Lassalle, *Geant: Simulation Program For Particle Physics Experiments. User Guide And Reference Manual*, *CERN Report* CERN-DD-78-2-REV (1978).

[38] M. Vanderhaeghen, P.A.M. Guichon and M. Guidal, *Deeply virtual electroproduction of photons and mesons on the nucleon: Leading order amplitudes and power corrections*, *Phys. Rev.* **D 60** (1999) 094017 [hep-ph/9905372] [INSPIRE].

JHEP01(2014)077